Appl Microbiol Biotechnol (2016) 100:5849–5858
DOI 10.1007/s00253-016-7391-1

Hierarchical nanostructures of Au@ZnO: antibacterial and antibiofilm agent

Haribhau Gholap[1] · **Sambhaji Warule**[2] · **Jaiprakash Sangshetti**[3] · **Gauri Kulkarni**[4] · **Arun Banpurkar**[4] · **Surekha Satpute**[4] · **Rajendra Patil**[5]

Received: 28 June 2015 / Revised: 21 January 2016 / Accepted: 11 February 2016 / Published online: 8 March 2016

Abstract The perpetual use of antibiotics against pathogens inadvertently altered their genes that have translated into an unprecedented resistance in microorganisms in the twenty-first century. Many researchers have formulated bactericidal and bacteriostatic inorganic nanoparticle-based antiseptics that may be linked to broad-spectrum activity and far lower propensity to induce microbial resistance than organic-based antibiotics. Based on this line, herein, we present observations on microbial abatement using gold-based zinc oxide nanostructures (Au@ZnO) which are synthesized using hydrothermal route. Inhibition of microbial growth and biofilm using Au@ZnO is a unique feature of our study. Furthermore, this study evinces antimicrobial and antibiofilm mechanisms of photo-eradiated Au@ZnO by disruption of cellular functions and biofilms via reactive oxygen species (ROS)-dependent generation of superoxide anion radical. The present study is significant as it introduces novel functionalities to Au@ZnO in the biomedical field which can be extended to other species of microbial pathogens.

Keywords Au@ZnO · Hydrothermal · Antimicrobial · Antibiofilm · ROS

Electronic supplementary material The online version of this article (doi:10.1007/s00253-016-7391-1) contains supplementary material, which is available to authorized users.

✉ Haribhau Gholap
haribhau.gholap@fergusson.edu

✉ Rajendra Patil
rpatil@unipune.ac.in

[1] Department of Physics, Fergusson College, Savitribai Phule Pune University, Pune 411004, India

[2] Department of Physics, Nowrosjee Wadia College, Savitribai Phule Pune University, Pune 411001, India

[3] Y. B. Chavan College of Pharmacy, Dr. Rafiq Zakaria Campus, Aurangabad 431001, India

[4] Department of Physics, Savitribai Phule Pune University, Pune 411007, India

[5] Department of Biotechnology, Savitribai Phule Pune University, Pune 411007, India

Introduction

The re-emergence of infectious diseases and the continuous development of antibiotic resistance amongst disease-causing microorganisms pose a serious threat to public health (McIntyre 2012). One of the reasons for this resistance has been the ability of these microorganisms to form a biofilm on surfaces. Biofilms are defined as conglomerations of microbial cells protected by a self-synthesized extra-polymeric substance (EPS) (Stewart and Costerton 2001). The EPS act as a diffusion barrier, restrict the entry of antibiotics inside the biofilm, and therefore, despite the antibiotics treatment, microorganisms survive in the biofilm, often leading to chronic infections (Bjarnsholt 2013). In the medical sector, up to 60 % of all human infections have implicated due to biofilm (Davies 2003). The biofilm formation has also caused a significant economic loss in the industrial sector (Van Houdt and Michiels 2010). In industry, biofilms have been implicated in the contamination of installations in the food industry by colonization of the interior of pipes. The yearly economic losses caused by "biofouling" (due to biofilm formations) in the marine industry were estimated at $6.5 billion (Yebra et al. 2004).

Recent advances in the field of nanotechnology, particularly the ability to manipulate the phase, size, shape, and functionality of inorganic, organic, and hybrid nanosystems, have led to the development of new "nanobiocidal" agents

(Stoimenov et al. 2002). There are countless reports on the biocidal nature of nanomaterial; however, semiconductor metal oxide nanoparticles outsmart over all existing nanocomposites due to excellent photon absorption property and efficient transport of photogenerated charge carriers (Prokopovich et al. 2011). One of the most important semiconductor metal oxide nanoparticles is a zinc oxide (ZnO) with wide band gap energy of 3.37 eV and large exciton binding energy (60 meV). ZnO nanomaterials have received increasing attention as an excellent candidate for photocatalytical killing of microbial growth because of their stability under harsh processing conditions (Lipovsky et al. 2013; Ma et al. 2013). The interaction of ZnO nanomaterial with light underlies many of its biocidal applications. When light (usually UV light) is absorbed by ZnO nanomaterial, the photoexcited nanomaterial stores energy by charge separation, creating electron–hole pairs and generating reactive oxygen species (ROS). The ROS eventually oxidizes organic matter and, thus, imparts biocidal property to ZnO (Sirelkhatim et al. 2015). But low photoenergy conversion efficiency of ZnO (probably because of their relatively low charge separation efficiency and fast recombination of charge carriers) (Tamaki et al. 2009) forced many scientists to improve the photocatalytic efficiencies in ZnO by suppression of the recombination of photogenerated electron–hole pairs. Such examples include SnO_2/ZnO, ZnO/In_2O_3, Pt/ZnO, ZnO/ZnS, Bi_2S_3/ZnO, ZnO/CdS (Li et al. 2013), CdS/CdSe (Murugadoss 2012), ZnO/CdS (Sahi and Chen 2013), CeF_3/ZnO (Salazar et al. 2011), ZnO/CdTe and ZnO/CdS (Shirakata 2013), ZnO/CdS/Cu(In, Ga)Se_2 (Chang et al. 2013), ZnO/CuO (Tamez et al. 2012), SnO_2–ZnO (Yang et al. 2013), CdS/ZnO (Dongguang et al. 2012), Ag/ZnO–C (Yu et al. 2013), Pt–ZnO (Zhang et al. 2012), and CdS/CdSe (Song et al. 2009).

In this regard, the occurrence of metal nanoparticles on the surface of semiconductor nanostructures is expected to change the optical and electronic properties of noble metal/metal oxide hybrid nanostructures by increasing the efficiency of charge carrier separation and extending light absorption and facilitating creation of electron/hole pairs induced by the surface plasmon resonance (SPR) effect (especially for Au and Ag) (Lee et al. 2011; Mubeen et al. 2013).

Therefore, in the present study, we have attempted to increase the photocatalytical efficiency of ZnO nanoparticles by conjugating Au in the ZnO nanoparticles and studied its biocidal and antibiofilm activities against model organisms.

Materials and method

Synthesis of ZnO nanostructure

Zinc nitrate hexahydrate (Zn $(NO_3)_2 \cdot 6H_2O$) and potassium hydroxide (KOH) were used as source chemicals for the synthesis of ZnO nanostructures by hydrothermal method. One millimole of Zn $(NO_3)_2.6H_2O$ and 5 mmol of KOH were dissolved into 100 mL aqueous solution, and mixture was immediately transferred into a Teflon-lined stainless steel autoclave (200 mL). The hydrothermal synthesis was carried out at two different reaction temperatures, 85 and 120 °C for 2 h durations. After completion of the reaction, product was washed with distilled water and dried in an oven at 70 °C.

Synthesis of Au@ZnO nanostructure

In a typical experiment, 1 mol of Zn $(NO_3)_2$.6H2O, 5 mmol of KOH, and 0.05 mmol of $HAuCl_4$ were dissolved into 100 mL aqueous solution and mixture was immediately transferred into a Teflon-lined stainless steel autoclave (200 mL). The hydrothermal synthesis was carried out at 120 °C for 2 h durations. After completion of the reaction, the product was washed with distilled water and dried in an oven at 70 °C.

Structural characterizations

ZnO and ZnO/CdTe nanostructures were characterized by X-ray powder diffraction (XRD) (Philips X'Pert PRO), field emission scanning electron microscopy (FESEM) (Hitachi S-4800), and high-resolution transmission electron microscopy (HRTEM) (FEI Tecnai 300). The optical properties were studied by ultraviolet–visible (UV–vis) spectroscopy (JASCO V-670 spectrophotometer), and photoluminescence (PL) spectroscopy measurements were performed on a Perkin-Elmer LS 55 spectrophotometer.

Antibacterial

It was performed by using model organisms, *Bacillus subtilis* NCIM 2063 and *Escherichia coli* NCIM 2931, in the presence of visible light (Fluorescence lamp 36 W, 2450 lm). It was performed by counting the number of viable cells as colony forming units per milliliter (CFU/mL). In short, approximately about 1×10^6 cells/mL of *B. subtilis* and *E. coli* were inoculated with Au@ZnO nanostructures (in the concentration range of 0 to 500 μg/mL), separately, and incubated at 37 °C for 15 h. After 15 h, viable numbers of cells were counted in comparison to control (without nanostructures). To observe the cellular morphologies of *B. subtilis* in the presence of Au@ZnO, SEM was performed. In short, the cells of *B. subtilis* were grown to mid-log phase (approximately 1×10^7 cells/mL) and treated with respective MIC concentration of Au@ZnO nanostructure for 3 h at 37 °C and 150 rpm. The cells were collected by centrifugation at 10,000*g* for 15 min at 4 °C. The pellets were then washed three times with 0.1 M phosphate buffer at pH 7.4 and fixed in 2.5 % glutaraldehyde at 4 °C for 4 h. After rinsing twice with buffer, the pellets were dehydrated in ethanol serials (10–100 %, 15 min

per step) and then dried in air. Finally, the images were seen under SEM (Joel JSM).

Antibiofilm

It was performed by using *Pseudomonas aeruginosa* MTCC 2297 by crystal violet retention assay. Crystal violet has an ability to absorb to polysaccharides of biofilm. In short, the *P. aeruginosa* was grown overnight in Luria Bertaini (LB) medium at 37 °C with agitation. After growth, the culture was diluted with LB medium (OD 600 = 0.02), and 50 μL of the diluted culture was added to 950 μL of LB medium and allowed to form biofilm. After the formation of biofilm on polystyrene plastic surfaces, the planktonic cells (suspended cells in the medium) were replaced with fresh medium each supplemented with 0–500 μg/mL of Au@ZnO nanostructures and incubated statically for 18 h at 37 °C. After incubation, planktonic bacteria were discarded and the biofilms were washed three times with phosphate buffered saline buffer. Washed biofilms were fixed with 1 mL of methanol (99 %). After 15 min, the methanol was discarded and the plates were dried at room temperature. Crystal violet (0.1 % in water) was then added to each well (1 mL/well), and the plates were incubated for 15 min at room temperature. Crystal violet was then discarded, and stained biofilms were washed three times with 1 mL of water. Acetic acid (33 % in water) was added to the stained biofilms (2 mL) in order to solubilize the crystal violet, and the absorbance of the solution was read at 590 nm with a spectroscopy (Shimadzu, Japan). Further, to observe the structure of the biofilm, SEM was performed. For SEM analysis, the biofilm was dehydrated in a series of ethanol solutions (10–100 %, each for 15 min). The biofilm was dried, mounted on aluminum stubs with conductive carbon cement, and finally coated with a gold film. The samples were observed under SEM (Joel JSM).

Results

X-ray diffraction study of ZnO and Au@ZnO

The observed peaks can be well indexed to the hexagonal wurtzite structure of bulk crystalline ZnO [JCPDS no. 36–1451] and the face-centered cubic structure of Au [JCPDS card no. 04–0784]. Appearance of Au peaks in the diffraction patterns clearly indicates the formation of crystalline Au nanoparticles on ZnO nanostructures. No extra peaks related to any impurities or silver oxides were observed, which confirms that the as-synthesized products are pure wurtzite ZnO and Au@ZnO nanostructures (Fig. 1).

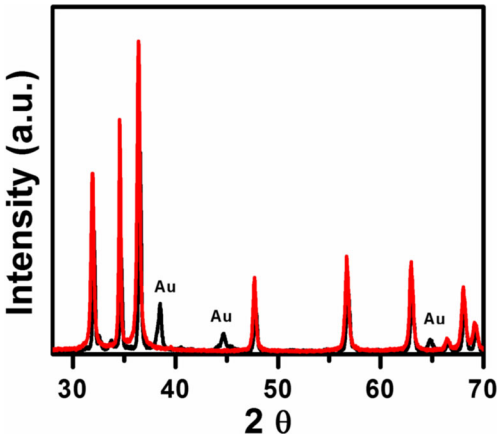

Fig. 1 X-ray diffraction of ZnO (*red in color*) and Au@ZnO nanostructure (*black in color*)

Optical properties of ZnO and Au@ZnO

The optical properties of ZnO and Au@ZnO samples were studies by UV–visible diffused reflectance (UV–vis-DRS) and photoluminescence spectroscopy at room temperature. The UV–vis–DRS of ZnO and Au@ZnO is shown in Fig. 2. It can be seen that Au@ZnO samples exhibit two prominent absorption peaks (380 and 570 nm). A strong broad band around 570 nm is due to Au. This band has been found to redshift, broaden, and increase in intensity with an increase in the extent of Au NPs loading onto ZnO nanostructures (data not shown). Room temperature PL spectrum of the ZnO sample excited by 350 nm UV light is shown in Fig. 3. The photoluminescence spectra of ZnO consists of three emission bands, a near-band-edge (UV) emission (393) and broad, deep-level (visible) emissions (598).

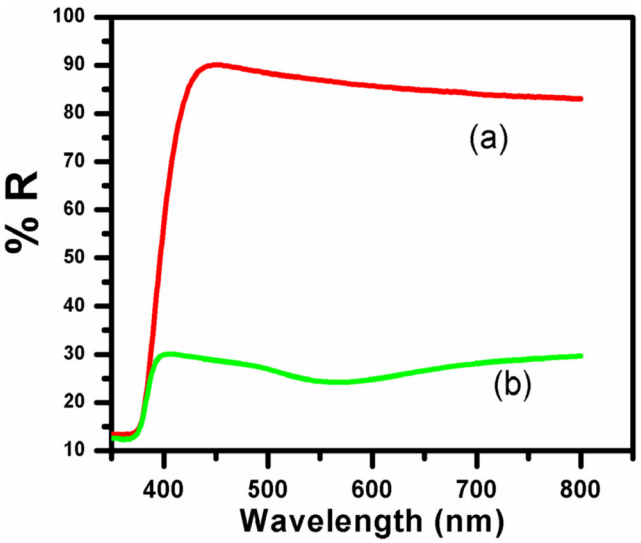

Fig. 2 UV–visible diffused reflectance of (*a*) ZnO and (*b*) Au@ZnO nanostructure

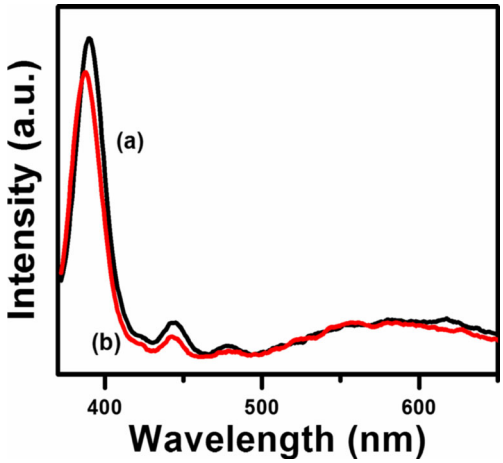

Fig. 3 Photoluminescence of ZnO (*black in color*) and Au@ZnO (*red color*)

Raman spectroscopy of ZnO and Au@ZnO

To investigate the influence of Au on the molecular vibrational modes of ZnO nanostructures, room temperature Raman spectra of ZnO and Au@ZnO samples in the spectral range of 100 to 800 cm^{-1} were measured (Fig. 4). The Raman spectra of pristine ZnO nanostructures were observed at 329 (second-order vibration), 379, 408, 435, 537, 579, 658, and 704 cm^{-1} corresponding to the E_{2H}-E_{2L}, A_1(TO), E_1 (TO), E_{2H}, TO + TA(M), E_1 (LO), and E_{2L}-B_{1H} fundamental phonon modes of hexagonal ZnO nanostructure, respectively. Au@ZnO nanostructure-related vibrational modes were identified as follows: 427, 489, 600, and 704 cm^{-1}. The main peak, 427 cm^{-1}, slightly redshifted to a lower wavenumber, 475 cm^{-1}. The redshift in the Au@ZnO nanostructures further confirms the size effect of quantum confinement.

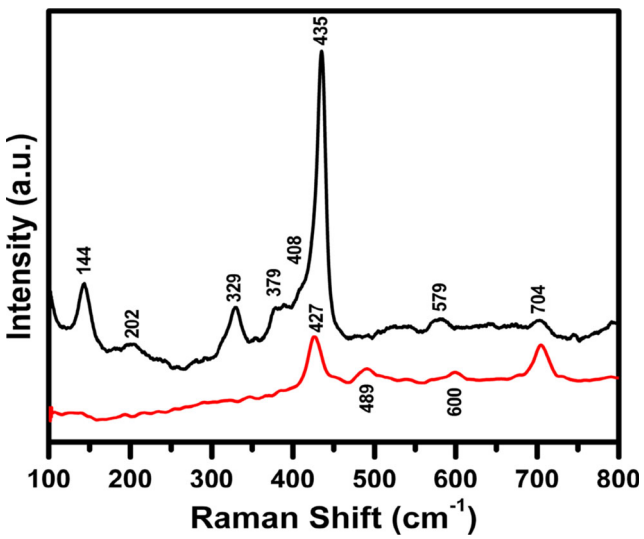

Fig. 4 Raman spectra of (*black*) ZnO and (*red*) Au@ZnO nanostructure

Structural morphology of ZnO and Au@ZnO

The structural morphologies of ZnO and Au@ZnO were observed under TEM and HRTEM (Figs. 5, 6, and 7). Under low-resolution TEM, ZnO and Au@ZnO were observed as flowerlike structures with a diameter of 1–2 μm and constructed by numerous nanosheets which have a uniform thickness of ~10 nm. The high-resolution TEM image of ZnO nanostructures (Figs. 5 and 7) clearly shows lattice fringes and the measured lattice spacing of 0.26 nm. The HRTEM image of Au@ZnO sample is shown in Fig. 7 and reveals lattice fringes of 0.24 and 0.26 nm which correspond to the (002) and (111) interplanar spacing (d-spacing) of Au and ZnO, respectively. Figure 7 shows the selected area diffraction (SAD) pattern from a region marked by a dotted circle. The SAD pattern shows concentric rings consisting of distinct spots, which is because of the presence of many small crystals and also suggests the crystalline nature of Au@ZnO nanostructures.

Antibacterial studies of Au@ZnO

All biological studies were performed under ordinary laboratory light. We have performed all biological studies using only Au@ZnO sample since our PL data shows that ZnO nanostructures do not show absorption under ordinary light, as opposed to Au@ZnO which showed absorption under ordinary light. The antibacterial study is shown in Fig. 8. We started our antibacterial study with approximately 4 to 5 Log CFU/mL of *B. subtilis* and *E. coli* (model organisms). As can be seen from Fig. 8, after 16 h of incubations, the growth of model organisms in the absence of nanomaterial was 8 to 9 Log CFU/mL (considered as 100 % growth). However, in the presence of Au@ZnO (20 μg/mL), the growth of *B. subtilis* decreased to 3 Log (99.9 % reduction of growth). However, a similar reduction was not observed for *E. coli*. Next, we decided to know the mechanism of action of Au@ZnO sample on *B. subtilis* by observing the cellular appearances of *B. subtilis* under SEM. When we observed the cellular morphology of *B. subtilis* in the presence of 20 μg/mL of Au@ZnO by SEM, we noted surface perturbation (pits and ruptured appearances) on the cell wall of *B. subtilis* (Fig. 9).

Antibiofilm studies of Au@ZnO

The antibiofilm activity of Au@ZnO nanostructures is as shown in Fig. 10. We assayed the biofilm formation/inhibition by measuring the amount of crystal violet retained by the biofilm. When the cells of *P. aeruginosa* were allowed to grow for 48 h, they tend to form biofilms on the surfaces of polystyrene plate, as revealed by the retention of the crystal violet. However, when *P. aeruginosa* was subjected to increasing concentration of the Au@ZnO sample, a reduction

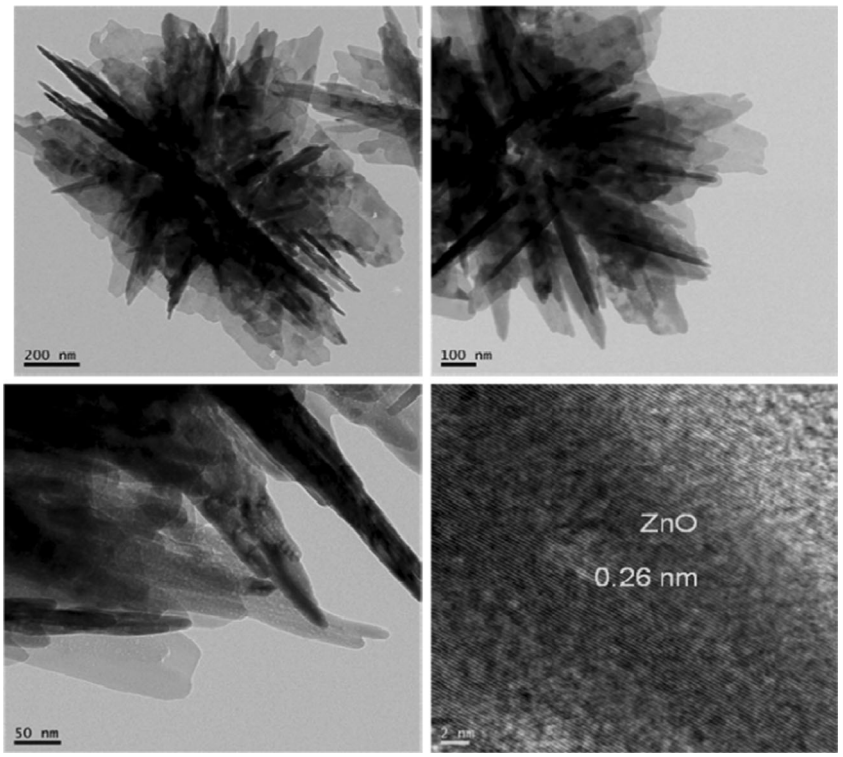

Fig. 5 TEM and HRTEM images of ZnO nanostructures

in the retention of crystal violet and hence decrease in the biofilm was observed (Fig. 10). At 31.25 μg/mL of Au@ZnO, a 29 % reduction in biofilm was observed. After 31.25 μg/mL, the decrease in biofilm was also associated with

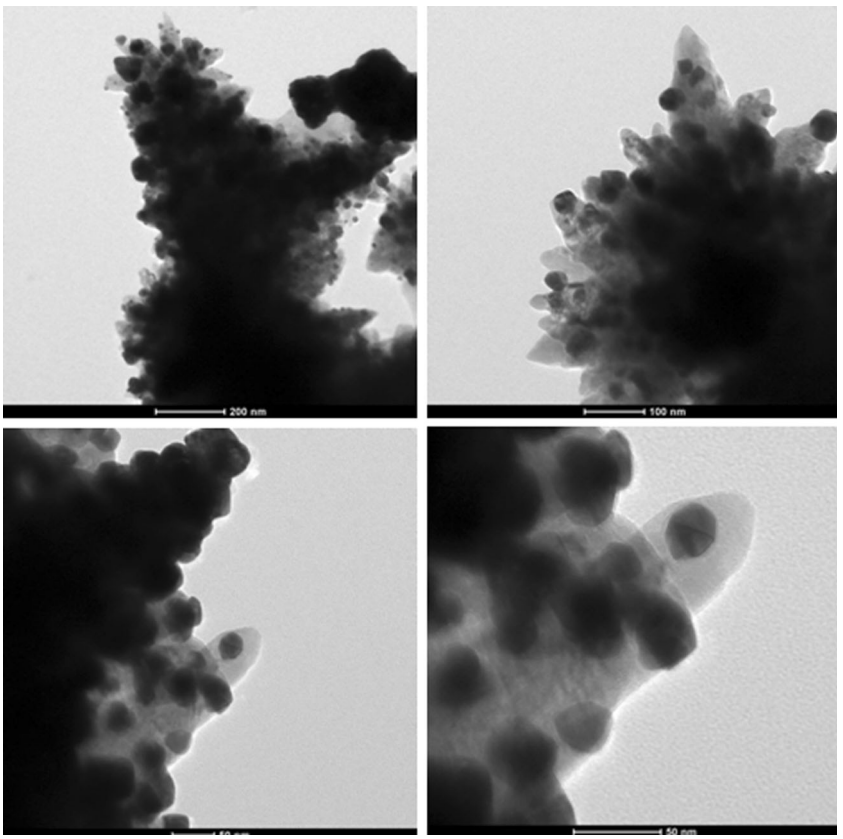

Fig. 6 TEM images of Au@ZnO nanostructures

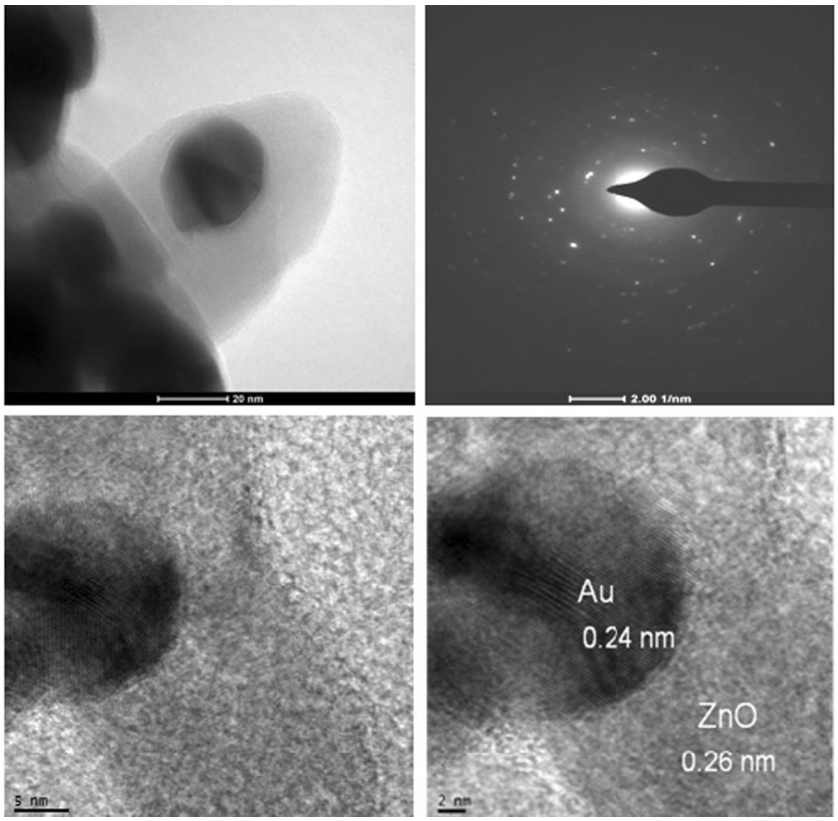

Fig. 7 TEM and HRTEM images of Au@ZnO flower-like nanostructure

the decrease in viable number of cells. In order to get the better idea of the extent of the biofilm inhibition, a topographical observation of biofilm was made under SEM. The biofilm of *P. aeruginosa* under SEM was observed as an intact structure of polysaccharide with cells inside (Fig. 11), a typical of biofilm structure. However, at 31.25 μg/mL of Au@ZnO, a truncated biofilm was observed.

Discussions

Characterizations of Au@ZnO

The XRD and UV–vis-DRS spectra characterized the synthesis of ZnO nanostructures and Au@ZnO nanostructures. In XRD, lattice constants (a = 0.325 nm and c = 0.521 nm; JCPDS: 36–1451) were well assigned to the crystal structure of ZnO, thus, confirming to the formation of ZnO nanostructure. The presence of peaks ($2\theta = 38.5°$) confirms the presence of Au nanocrystals on the surface of ZnO nanostructure. The absence of any other peak demonstrates the purity of the synthesized nanoparticles and nanostructures. In UV–vis-DRS spectroscopy, a peak around 380 nm is attributed to the excitonic absorption peak of ZnO nanostructure (Deng et al. 2012), and a peak around 570 nm is due to the growth of Au NPs on the surface of ZnO nanostructures. It was also observed that the intensity of UV emission decreased with an increase in the Au content of the samples. The decrease of intensity in the UV region clearly indicates that the recombination of electrons and holes was suppressed (Liu et al. 2004) which, in turn, improved the photocatalytic destruction of microbial cells and biofilm. In UV–vis-DRS spectroscopy, the peak at 570 been found to redshift, broaden, and increased in intensity due to the SPR peak of Au nanoparticles (Wang et al. 2010). It is known that the SPR wavelength of noble metal nanoparticles can be tuned by tailoring the size, shape, interparticle spacing, and surrounding medium (Kelly et al. 2003). In PL spectra, a peak near-band-edge emission (393 nm) results from the recombination of free excitons (Zhou et al. 2007), a weak emission peak at 440 nm (blue emission) results due to surface defect in ZnO, mainly due to Zn vacancy (Dutta and Ganguly 2012), and a strong emission at 598 nm in the yellow region results from various intrinsic defects in ZnO nanostructures. Normally, these defects are located on the surface of the ZnO nanostructures (Li et al. 2009; Wu et al. 2001).

In Raman spectra, the 329-cm^{-1} mode was observed due to the enhancement of Raman active and inactive phonons. The 379-cm^{-1} mode lifted the degeneracy of infrared active optical phonons into a transverse (TO) branch. The 408-cm^{-1} mode is associated with lattice disorder along the c-axis of the ZnO crystal; the 435-cm^{-1} mode corresponds to E_2 mode of wurtzite ZnO. The 579-cm^{-1} E_1(LO) corresponds to well resolve Raman peak due to multiphonon and resonance processes and are related to oxygen deficiency.

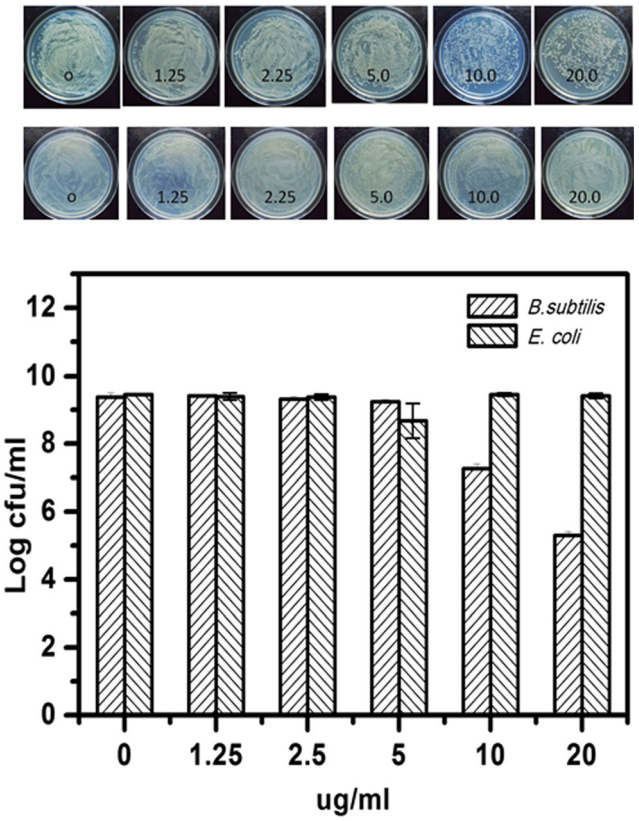

Fig. 8 Determination of minimum bactericidal concentration of Ag@ZnO nanostructure: (*upper*): photographic representation of the antibacterial activity of nanostructure against *B. subtilis* and *E. coli*. (*Lower*) the cultures were set up at an initial conc of 1×10^5 in Muller Hinton broth containing various concentrations (1.25–20 μg/mL) of Au@ZnO nanostructures and incubated for 12 h at 180 r.p.m. and 37 °C. A 3 Log reduction in the number of viable cells of *B. subtilis* occurred at 20 μg/mL, while there was no effect of Au@ZnO on cells of *E. coli*, in comparison to control, under similar conditions. *Error bars* represent the standard deviation ($n = 3$)

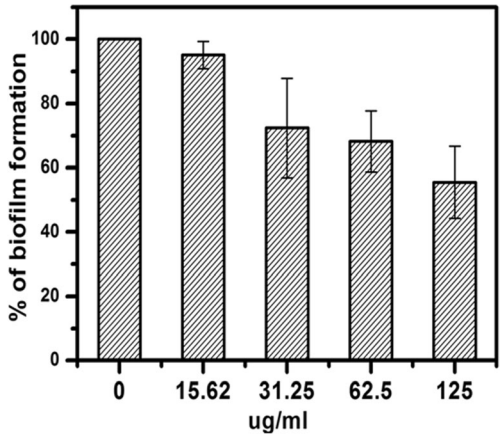

Fig. 10 Effect of Ag@ZnO nanostructure on biofilm: The cultures of *P aeruginosa* were set up at initial inoculums of 1×10^6 in Luria Bertaini broth and incubated at 37 °C in the presence of various concentration of Au@ZnO nanostructure. After the removal of planktonic cells, formed biofilm was treated with 0.1 % crystal violet and extracted in acetic acid to read at 595 nm. At 31.25 μg/mL of nanostructure, there was a reduction in biofilm by about approx. 29 %. Above this conc., there was a decrease in the number of viable cells. *Error bars* represent the standard deviation ($n = 3$)

Antibacterial activity of Au@ZnO

The microbial resistance to antibiotics poses a serious threat to public health worldwide (Sriramulu 2013). Many strategies were developed to design appropriate antimicrobial agents which will not only kill these drug-resistant pathogens but also will not induce resistance in such pathogens. Unlike the organic agents whose indiscriminate use induced a drug resistance, inorganic antimicrobial materials are not likely to induce the drug resistance since multiple simultaneous gene mutations should occur in such cells, which is yet not reported. Therefore, in the last few years, an interest in nanomaterial synthesis has gained momentum (Chernousova and Epple 2013; Lipovsky et al. 2013; Pelgrift and Friedman 2013). Because of unique properties of ZnO nanoparticles viz. good thermal stability (which helped in the synthesis of ZnO nanostructure by various methods) and non-toxicity (Colon et al. 2006), in the present study, we explored the functionality of Au@ZnO nanostructures to eradicate microbial growth and biofilm.

The pronounce action of ZnO nanostructures on *B. subtilis* seems due to the difference in the cell wall composition between these *B. subtilis* and *E. coli*. Most of the Gram-negative

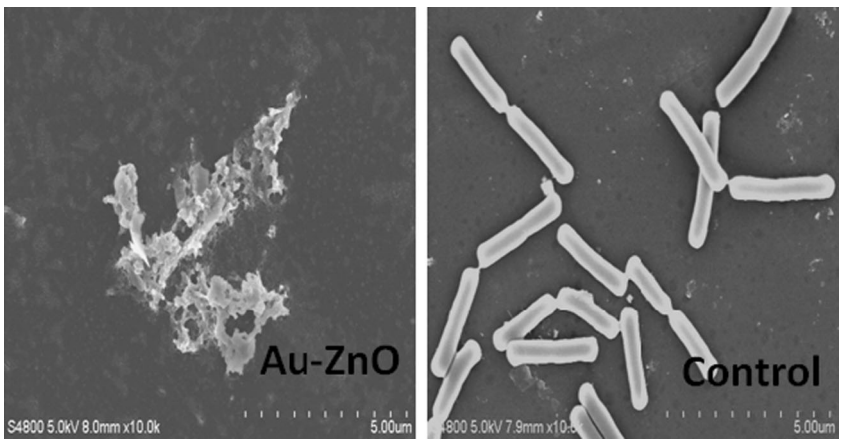

Fig. 9 Effect of Ag@ZnO nanostructure on cellular morphology: The cell surface morphology of *B. subtilis* in the presence of Au-ZnO nanostructures at MIC value for 4 h at 37 °C and 180 r.pm. showed a ruptured appearance of cells of *B. subtilis* (*left*) and *E. coli* (*right*) in comparison to controls

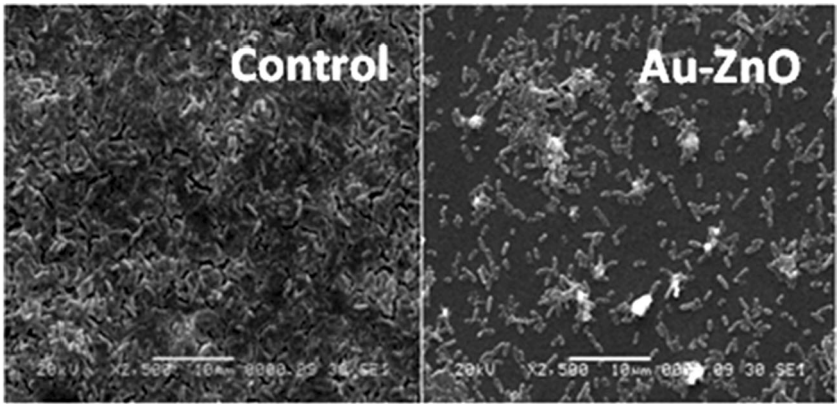

Fig. 11 Effect of Ag-ZnO nanostructure on biofilm structure: Cells of *P. aeruginosa* (mid log phase, approx. 1×10^5 cells/mL) in presence sub-inhibitory conc. of Au@ZnO nanostructures were seen as sparsely distributed without the associated matrix as opposed to control wherein they were observed as compact mass of structures surrounded by biofilm matrix

organisms, including *E. coli*, possess an extra outermost layer made up of lipopolysaccharide and thus may restrict the damage to cell membrane of organisms (Wagh et al. 2013). The antibacterial action of Au@ZnO nanostructures can be explained in the light of following four most common reported mechanisms: (1) the uptake of free Ag ions followed by the disruption of ATP production and DNA replication (Chernousova and Epple 2013), (2) the charging-discharging model for superoxide-mediated generation of reactive oxygen species (ROS) (He et al. 2011), (3) the Ag NPs and Ag ions generation of ROS (Xu et al. 2012), and (4) the Ag nanoparticles direct damage to the cell membranes (Gholap et al. 2013; Panmand et al. 2014). In our previous study (Patil et al. 2015; Patil et al. 2014), we have shown that ZnO nanostructures act on microbial cells by generating ROS on cellular membrane, which virtually oxidizes every cellular components and thus ruptures the cell wall. Therefore, in the present study, we hypothesize that the electrostatic interactions between Au@ZnO nanostructures and bacterial cells might have recruited the former on cellular surfaces of *B. subtilis*, and a series of the oxidative reactions (explained in following section) would have brought about the observed antibacterial effect. This hypothesis was tested by observing the cellular morphologies of *B. subtilis* under SEM. When we observed the cellular morphology of *B. subtilis* under SEM, we observed the surface perturbation, in agreement with the previous reports (Gholap et al. 2013; Panmand et al. 2014). This is also supported by a recent study (He et al. 2014) and Wang et al. (2015) wherein the photogenerated charge carriers and reactive oxygen species in ZnO/Au hybrid nanostructures were reported for antibacterial activities.

Antibiofilm activity of Au@ZnO

Next, we moved to study the effect of Au@ZnO nanostructures on the biofilm of *P. aeruginosa*. The most characteristic phenotype of the biofilm mode of growth is its inherent resistance to antimicrobial treatment and immune response killing (de la Fuente-Nunez et al. 2013). The medical implants and indwelling devices are severely affected due to bacterial colonization and biofilm formation. Thus, conventional antibiotic therapies which were effective against device-associated biofilm now are falling without the removal of the infected implant (Sun et al. 2013). Recently, nanostructures have been effectively shown to inhibit. For example, Campoccia et al. (2013) synthesized classes of bacteria repelling and anti-adhesive surfaces on nanomaterials to inhibit bacterial biofilm, De Faria et al. (2014) has decorated Ag NPs on graphene oxide (GO) nanosheets and showed an antibiofilm activities, Durmus et al. (2013)) have shown an improved efficacy vancomycin with superparamagnetic iron oxide particles by manipulating the biofilm metabolic microenvironment, Inbakandan et al. (2013)) showed efficacy of Ag NPs on marine biofilm-forming bacterial species, Ronen et al. (2013)) reconstructed commercial polypropylene feed spacer with composite spacer containing zinc oxide nanostructures to repress biofilm development on membranes, Taglietti et al. (2014)) designed a glass surface modified with AgNPs and showed biofilm inhibition in *Staphylococcus epidermidis*. However, in comparison to all these various reports, the present work is significant because (i) Au@ZnO nanostructures are relatively non-toxic and (ii) Au@ZnO nanostructures not only have inhibited the biofilm but also have reduced the viability of cells as well, which is important because if cells in the biofilm are not viable, they will not form biofilm and, thus, the biofilm would be permanently eradicated.

Although there are no concrete studies on the mechanism of inhibition of biofilm by the nanoparticles, we hypothesize that the antibiofilm of Au@ZnO nanostructures could be due to interaction of nanostructures with the polymeric substances of biofilm. There are few reports in support of this hypothesis (Gholap et al. 2013; Wagh et al. 2013; Radzig et al. 2013). In our antibacterial study, since a reporter of ROS on cellular surfaces was hypothesized for the microbial destructions, the biofilm inhibition of *P. aeruginosa*, therefore, could occur due to a similar photocatalytic generation of ROS. Since histidine has been shown to play an important role in the oxidative stress in *P. aeruginosa* (Lemire et al. 2010), we have

performed a supporting experiment (Supplementary Fig. S1). In this experiment, when we observed the biofilm structure in the presence of Au@ZnO and histidine (an antioxidant), we found an increase in the formation of biofilm in comparison to one observed in the presence of 31.25 μg/mL of Au@ZnO. In other words, the histidine alleviated the effect of ROS and restored the biofilm formation in *P. aeruginosa*, thus proving the observation that generation of ROS by Au@ZnO is responsible for the antibiofilm activity. In the presence of aqueous solution and upon irradiation of Au@ZnO nanostructures, electrons in the valence band are excited and promoted across the band gap to the conduction band, which create a hole in the valence band. Electrons in the conduction band and holes in the valence band exhibited high reducing and oxidizing power, respectively, and result in generation of ROS. The valence band-edge energy and conduction band-edge energy of semiconductors determine the type of ROS generated during photoexcitation. The redox potential for dissolved oxygen/superoxide couple is −0.16 V ($E_0(O_2(aq)/O2^{-\bullet})$) and for the H_2O/OH couple is 2.32 V($E_0(H_2O/\cdot OH)$) at pH 7.40. Therefore, photogenerated electrons, needed to form superoxide, must therefore have a potential less than −0.16, and photogenerated holes, needed to form hydroxyl radicals, must have a potential greater than 2.32. A wide band gap (Eg = 3.2 eV) semiconductor such as ZnO has a conduction band edge with a redox potential of −0.2 V and a valence band edge with a redox potential of 3.0 V. Thus, the highly reactive holes react with water to generate hydroxyl radicals, and electrons react with dissolved oxygen to produce superoxide anions. We hypothesize that more hydroxyl radicals are generated than superoxide anions during photoexcitation of Au@ZnO nanostructures. This may be attributed to the higher redox potential difference (0.68 V) between the valence band edge and the $H_2O/\cdot OH$ couple than those (0.04 V) between the conduction band electrons and $O_2(aq)/O_2^{-\bullet}$.

Thus, the daunting task of the twenty-first century (antimicrobial resistance) has necessitated the search for the synthesis of ZnO and Au@ZnO nanostructures, and in this endeavor, Au@ZnO nanostructures have proved worth as an alternative to organic-based drugs. The antibacterial and antibiofilm in the present study warrants the successfulness of the as-synthesized nanostructures in antimicrobial therapies. The ruptured appearances on cell surfaces and truncated biofilm further elaborate the mechanisms of action of Au@ZnO nanostructures.

Acknowledgments Haribhau Gholap acknowledges research funding from the Board of College and University Development (BCUD), Savitribai Phule Pune University, and Fergusson College, Pune, India, for the research facility. Rajendra Patil acknowledges UPE-II phase grant and Departmental Research and Development Grant, Department of Biotechnology, Savitribai Phule Pune University, for the financial support. We are thankful to Dr. Satishchandra Ogale (Scientist G), National Chemical Laboratory and Dr. Kale Bharat (Scientist F), C-MET, Pune, for the help and support.

Compliance with ethical standards This article does not contain any studies with human participants or animals performed by any of the authors.

Conflict of interest The authors declare that they have no competing interests.

References

Bjarnsholt (2013) The role of bacterial biofilms in chronic infections. APMIS Suppl 136:1–51

Campoccia D, Montanaro L, Arciola C (2013) A review of the biomaterials technologies for infection-resistant surfaces. Biomaterials 34: 8533–8554

Chang T, Li Z, Yun G, Jia Y, Yang H (2013) Enhanced photocatalytic activity of ZnO/CuO nanocomposites synthesized by hydrothermal method. Nano-Micro Lett 5:163–168

Chernousova S, Epple M (2013) Silver as antibacterial agent: ion, nanoparticle, and metal. Angew Chem Int Ed 52:1636–1653

Colon G, Ward B, Webster T (2006) Increased osteoblast and decreased *Staphylococcus epidermidis* functions on nanophase ZnO and TiO_2. J Biomed Mater Res A 78:595–604

Davies D (2003) Understanding biofilm resistance to antibacterial agents. Nat Rev Drug Discov 2:114–122

De Faria A, Martinez D, Meira S, De Moraes A, Brandelli A, Filho A, Alves O (2014) Anti-adhesion and anti-bacterial activity of silver nanoparticles supported on graphene oxide sheets. Colloids Surf B 113:115–124

de la Fuente-Nunez C, Reffuveille F, Fernandez L, Hancock R (2013) Bacterial biofilm development as a multicellular adaptation: antibiotic resistance and new therapeutic strategies. Curr Opin Microbiol 16:580–589

Deng Q, Duan X, Ng DHL, Tang H, Yang Y, Kong M, Wu Z, Cai W, Wang G (2012) Ag nanoparticle decorated nanoporous ZnO microrods and their enhanced photocatalytic activities. ACS Appl Mater Inter 4:6030–6037

Dongguang Y, Le Z, Binhu L, Minghong W (2012) Ag/ZnO-C nanocomposite-preparation and photocatalytic properties. J Nanosci Nanotechnol 12:2248–2253

Durmus N, Taylor E, Kummer K, Webster T (2013) Enhanced efficacy of superparamagnetic iron oxide nanoparticles against antibiotic-resistant biofilms in the presence of metabolites. Adv Mater 25: 5706–5713

Dutta S, Ganguly B (2012) Characterization of ZnO nanoparticles grown in presence of folic acid template. J Nanobiotechnol 10:29

Gholap H, Patil R, Yadav P, Banpurkar A, Ogale S, Gade W (2013) CdTe–TiO_2 nanocomposite: an impeder of bacterial growth and biofilm. Nanotechnology 24:195101

He D, Jones A, Garg S, Pham A, Waite T (2011) Silver nano-particle reactive oxygen species interactions: application of a charging–discharging model. J Phys Chem C 115:5461–5468

He W, Kim H, Wamer W, Melka D, Callahan J, Yin J (2014) Photogenerated charge carriers and reactive oxygen species in ZnO/Au hybrid nanostructures with enhanced photocatalytic and antibacterial activity. J Am Chem Soc 136:750–757

Inbakandan D, Kumar C, Abraham L, Kirubagaran R, Venka-tesan R, Khan S (2013) Silver nanoparticles with anti microfouling effect: a study against marine biofilm forming bacteria. Colloids Surf B 111: 636–643

Kelly K, Coronado E, Zhao L, Schatz G (2003) The optical properties of metal nanoparticles: the influence of size, shape, and dielectric environment. J Phys Chem B 107:668–677

Lee J, Shim H, Lee M, Song K, Dongil D (2011) Size-controlled electron transfer and photocatalytic activity of ZnO-Au nanoparticle composites. J Phys Chem Lett 2:2840–2845

Lemire J, Milandu Y, Auger C, Bignucolo A, Appanna P, Appanna D (2010) Histidine is a source of the antioxidant, alpha-ketoglutarate, in *Pseudomonas fluorescens* challenged by oxidative stress. FEMS Microbiol Lett 309:170–177

Li Y, Feng H, Zhang N, Liu C (2009) Hydrothermal synthesis and characterization of tube-structured ZnO needles. Mater Sci Poland 27: 551–557

Li C, Yang L, Xiao J, Wu Y, Søndergaard M, Luo Y, Li D, Meng Q, Iversen B (2013) ZnO nanoparticle based highly efficient CdS/CdSe quantum dot-sensitized solar cells. Phys Chem Chem Phys 15: 8710–8715

Lipovsky A, Gedanken A, Lubart R (2013) Visible light-induced antibacterial activity of metal oxide nanoparticles. Photomed Laser Surg 31: 526–530

Liu X, Wu X, Cao H, Chang R (2004) Growth mechanism and properties of ZnO nanorods synthesized by plasma-enhanced chemical vapor deposition. J Appl Phys 95:3141–3147

Ma H, Williams P, Diamond S (2013) Ecotoxicity of manufactured ZnO nanoparticles—a review. Environ Pollut 172:76–85

McIntyre R (2012) Common nanomaterials and their use in real world applications. Sci Prog 95:1–22

Mubeen S, Lee J, Singh N, Krämer S, Stucky G, Moskovits M (2013) Autonomous photosynthetic device in which all charge carriers derive from surface plasmons. Nat Nanotechnol 8:247–251

Murugadoss G (2012) ZnO/CdS nanocomposites: synthesis, structure and morphology. Particuology 10:722–728

Panmand R, Patil R, Kale B, Nikam L, Kulkarni M, Thombre D, Gade W, Gosavi S (2014) Self assembly of nanostructured hexagonal cobalt dendrites: an efficient anti-coliform agent. RSC Adv 4:4586–4595

Patil S, Patil R, Kale S, Tamboli M, Ambekar J, Gade W, Kolekar S, Kale B (2014) Nanostructured microspheres of silver @ zinc oxide: an excellent impeder of bacterial growth and biofilm. J Nanoparticle Res 16:2717

Patil R, Gholap H, Warule S, Banpurkar A, Kulkarni G, Gade W (2015) Quantum dots conjugated zinc oxide nanosheets: impeder of microbial growth and biofilm. Appl Surf Sci 326:73–81

Pelgrift R, Friedman A (2013) Nanotechnology as a therapeutic tool to combat microbial resistance. Adv Drug Deliv Rev 65:1803–1815

Prokopovich S, Pratten J, Parkin I, Wilson M (2011) Nanoparticles: their potential use in antibacterial photodynamic therapy. Photochem Photobiol Sci 10:712–720

Radzig M, Nadtochenko V, Koksharova O, Kiwi J, Lipasova V, Khmel I (2013) Antibacterial effects of silver nano-particles on gram-negative bacteria: influence on the growth and biofilms formation, mechanisms of action. Colloids Surf B 102:300–306

Ronen A, Semiat R, Dosoretz C (2013) Impact of ZnO embedded feed spacer on biofilm development in membrane systems. Water Res 47: 6628–6638

Sahi S, Chen W (2013) Luminescence enhancement in CeF_3/ZnO nanocomposites for radiation detection. Radiat Meas 59:139–143

Salazar R, Delamoreanu A, Lévy Clément C, Ivanova V (2011) ZnO/CdTe and ZnO/CdS core shell nanowire arrays for extremely thin absorber solar cells. Energy Procedia 10:122–127

Shirakata S (2013) Photoluminescence characterization of photovoltaic effect in ZnO/CdS/Cu (In, Ga) Se2 heterostructure. Phys Status Solid A 210:1322–1327

Sirelkhatim A, Mahmud S, Seeni A, Kaus NHM, Ann L, Bakhori S, Hasan H, Mohamad D (2015) Review on zinc oxide nanoparticles: antibacterial activity and toxicity mechanism. Nano-Micro Lett 7(2): 219–242. doi:10.1007/s40820-015-0040-x

Song Y, Cao X, Guo Y, Chen P, Zhao Q, Shen G (2009) Fabrication of mesoporous CdTe/ZnO@SiO_2 core/shell nanostructures with tunable dual emission and ultrasensitive fluorescence response to metal ions. Chem Mater 21:68–77

Sriramulu D (2013) Evolution and impact of bacterial drug resistance in the context of cystic fibrosis disease and nosocomial settings. Microbiol Insights 6:29–36

Stewart P, Costerton J (2001) Antibiotic resistance of bacteria in biofilms. Lancet 358:135–138

Stoimenov P, Klinger R, Marchin G, Klabunde K (2002) Metal oxide nanoparticles as bactericidal agents. Langmuir 18:6679–6686

Sun F, Qu F, Ling Y, Mao P, Xia P, Chen H, Zhou D (2013) Biofilm-associated infections. Future Microbiol 8:877–886

Taglietti A, Arciola C, D'Agostino A, Dacarro G, Montanaro L, Campoccia D, Cucca L, Vercellino M, Poggi A, Pallavicini P (2014) Antibiofilm activity of a monolayer of silver nanoparticles anchored to an amino-silanized glass surface. Biomaterials 35: 1779–1788

Tamaki Y, Hara K, Katoh R, Tachiya M, Furub A (2009) Femtosecond visible-to-IR spectroscopy of TiO_2 nanocrystalline films: elucidation of the electron mobility before deep trapping. J Phys Chem C 113: 11741–11746

Tamez M, Nicolas Y, Oliviér C, Toupance T, Servant L, Müller M, Kleebe H, Ziegler J, Jaegermann (2012) Nanostructured SnO_2–ZnO heterojunction photocatalysts showing enhanced photocatalytic activity for the degradation of organic dyes. Inorg Chem 51:7764–7773

Van Houdt R, Michiels C (2010) Biofilm formation and the food industry, a focus on the bacterial outer surface. J Appl Microbiol 109:1117–1131

Wagh M, Patil R, Kale S, Thombre D, Gade W, Kulkarni M, Kale B (2013) Evaluation of anti-quorum sensing activity of silver nanowires. Appl Microbiol Biotechnol 97:3593–3601

Wang R, Wang X, Xin J (2010) Advanced visible-light-driven self-cleaning Cotton by Au/TiO_2/SiO_2 photocatalysts. ACS Appl Mater Inter 2:82–85

Wang Y, Fang H-B, Zheng Y-Z, Ye R, Tao X, Chenb J-F (2015) Controllable assembly of well-defined monodisperse Au nanoparticles on hierarchical ZnO microspheres for enhanced visible-light-driven photocatalytic and antibacterial activity. Nanoscale 7:19118–11912

Wu X, Siu G, Fu C, Ong H (2001) Photoluminescence and cathodoluminescence studies of stoichiometric and oxygen-deficient ZnO films. Appl Phys Lett 78:2285

Xu H, Qu F, Xu H, Lai W, Wang Y, Aguilar Z, Wei H (2012) Role of reactive oxygen species in the antibacterial mechanism of silver nanoparticles on *Escherichia coli*. Biometals 25:45–53

Yang G, Yan W, Zhang Q, Shen S, Ding S (2013) One-dimensional CdS/ZnO core/shell nanofibers via single-spinneret electrospinning: tunable morphology and efficient photocatalytic hydrogen production. Nanoscale 5:12432–12439

Yebra D, Kiil S, Dam-Johansen K (2004) Antifouling technology—past, present and future steps towards efficient and environmentally friendly antifouling coatings. Prog Org Coat 50:75–104

Yu C, Yang K, Xie Y, Fan Q, Yu J, Shua Q, Wang C (2013) Novel hollow Pt-ZnO nanocomposite microspheres with hierarchical structure and enhanced photocatalytic activity and stability. Nanoscale 5:2142–2151

Zhang R, Luo Q, Chen H, Yu X, Kuang D, Su C (2012) CdS/CdSe quantum dot shell decorated vertical ZnO nanowire arrays by spin-coating-based SILAR for photoelectrochemical cells and quantum-dot-sensitized solar cells. Chem Phys Chem 13:1435–1439

Zhou J, Zhao F, Wang Y, Zhang Y, Yang L (2007) Size-controlled synthesis of ZnO nanoparticles and their photoluminescence properties. J Luminenescence 122:195–197